Condition Analysis of Expansion Joints of a Long-Span Suspension Bridge through Metamodel-based Model Updating Considering Thermal Effect

Qi Xia[1], Yong Xia[1], Hua-Ping Wan[2*], Jian Zhang[3], Wei-Xin Ren[4]

[1]*Department of Civil and Environmental Engineering, The Hong Kong Polytechnic University, Hong Kong, China*

[2]*College of Civil Engineering and Architecture, Zhejiang University, Hangzhou, China*

[3]*Jiangsu Key Laboratory of Engineering Mechanics, Southeast University, Nanjing, China*

[4]*College of Civil and Transportation Engineering, Shenzhen University, Shenzhen, China*

Summary

Expansion joints of bridges are vulnerable to damage due to the thermal expansion and contraction, vehicle traffic, etc. Currently, the temperature-displacement relationship model may be only qualitative method for condition evaluation of bridge expansion joints using the field monitoring data. The quantitative assessment based on the finite element model (FEM) updating techniques is heavy computational burden and time-consuming. Therefore, a Gaussian process (GP) metamodel-based model updating method is proposed in this study, and performed for the quantitative identification on the boundary condition of the expansion joints of Jiangyin Suspension Bridge using the long-term displacement and temperature monitoring data. At first, the relationship between the longitudinal boundary stiffness (LBS) and structural temperature is formulated on the basis of thermal effects of the bridge deck. The range of LBS is approximately estimated by the regression coefficients from one-year monitoring data and is used as initial bounds for the subsequent model updating procedure. The GP metamodel is formulated to map the relationship between the LBS and the longitudinal

*Corresponding author.

E-mail address: q.xia@polyu.edu.hk (Q. Xia); ceyxia@polyu.edu.hk (Y. Xia); hpwan@zju.edu.cn (H.-P. Wan); jian@seu.edu.cn (J. Zhang); renwx@szu.edu.cn (W.-X. Ren).

displacements under the thermal effects. The LBS identification of the Jiangyin Suspension Bridge is performed within the fast-running GP metamodel. The results show that the longitudinal displacements using the updated LBS are in good agreement with the measurements, which verifies the effectiveness of GP metamodel-based model updating method in identifying the LBS of the long-span suspension bridge.

KEYWORDS: expansion joints, boundary stiffness, thermal effect, Gaussian process metamodel, structural health monitoring

1 Introduction

Bridge expansion joints are designed to accommodate expansion and contraction of the bridge resulting from a variety of factors such as thermal effect, concrete shrinkage, creep, live loading, settlement of the foundation and substructure, and environmental variations [1-7]. Effective functioning of expansion joints is not only required for smooth traffic but also for ensuring bridge performance in extreme events, such as earthquakes and hurricanes. In practice, expansion joints are more vulnerable to damage than other bridge components. Damage in expansion joints may cause variation in structural dynamic and static properties. For example, Fu and DeWolf [8] pointed out that the natural frequencies of a two-span skewed composite bridge changed due to the damaged bearings. Xu et al. [9] found that the measured first natural frequency was 10% higher than the theoretical counterpart and explained that this difference was caused by the unclear understanding of the boundary conditions. Moreover, severe damage of expansion joints may restrain the movement of the bridge, generating large internal forces and causing damage to the bridge [10]. Kromanis et al. [11] found that the transversal temperature gradient of the Cleddau bridge caused plan-bending of the box girder and led to

degradation of the bearing.

The development of structural health monitoring (SHM) enables to gain insight into the performance of expansion joints during operation using the long-term monitoring data. Xia et al. [12] studied the thermal effects on a large-span suspension bridge using one-year monitoring data and found that the damaged expansion joints produced restraining internal forces on the main girder. Ni et al. [13] established the normal correlation pattern between the effective temperature and the expansion joints movement of the Ting Kau Bridge using the long-term displacement and temperature measurement, allowing for condition assessment of the bridge expansion joints. Ding and Li [14] found that temperature variation was the major factor of the expansion joint displacement. In addition, they used a mean value control chart to characterize the residual displacement for performance alarming of bridge expansion joints. Guo et al. [15] decomposed expansion joint displacement measurements into various frequency bands and revealed that the temperature-induced movements mainly contributed to displacement fluctuation whereas the wind and vehicle loads largely contributed to total cumulative displacement. Li and Sun [16], Huang et al. [17] and Winkler et al. [18] formulated the relation between temperature and displacement of bridge expansion joints and used it for assessing the performance of the expansion joints.

The above studies of the temperature-displacement relationship model are the qualitative methods for condition evaluation of bridge expansion joints. In recent years, the quantitative assessment of the boundary condition (e.g., restraint stiffness/force) of bridges has received an increasing interest. Yarnold et al. [19] identified the boundary stiffness of the expansion bearings of a steel arch bridge using a temperature-based model updating procedure. Murphy and Yarnold [20] demonstrated the capability of the temperature-based structural identification scheme in calibrating

the boundary condition parameters of a Route 61 Bridge. Zhou and Song [21] proposed a FEM updating method for structural identification of a pedestrian bridge with consideration of environmental effects. However, these studies focused on the simple structures. Jesus et al. [22, 23] applied a modular Bayesian model updating method to identify the boundary condition of a scaled aluminum bridge and a suspension bridge subjected to either thermal effect only or both temperature and traffic load effects. The importance of the definition reasonable boundaries is pointed out in this study. Xia et al. [24] theoretically derived the LBS identification method for a long-span suspension bridge based on temperature-induced effects. This study can be used to determine the initial bounds based on the long-term monitoring data.

Although the model updating technique has been developed to identify the boundary stiffness of bridges, some issues, such as initial boundary stiffness bounds, accurate thermal analysis, and efficient model updating method, still exist, especially for the long-span bridges. First, unreasonable initial bounds may cause the obtained results to lose physical meaning. However, these initial bounds are not strictly defined in the above literatures on the model updating. Second, large-scale bridges such as long-span suspension bridges generally have a complicated geometric configuration. The temperature at each differently oriented member may vary at different times. It is very difficult to accurately predict the detailed temperature distribution over the entire bridge using the simplified or scaled model. The refined 3D FEMs are essential for performing accurate thermal analysis. Third, the traditional FEM updating technique cannot be well performed under the thermal analysis of the refined 3D FEM because it requires a lot of calculation and time-consuming. So, the GP metamodel is utilized in this paper.

In this study, Jiangyin Suspension Bridge is used as a test example for the boundary condition identification. This paper is organized as follows: In Section 2, the SHM system of Jiangyin Suspension Bridge and its sensor layout are briefly introduced. The regression analysis between the longitudinal displacements of the expansion joints and the structural temperature is performed. In Section 3, the LBS of the expansion joints is formulated on the basis of the thermal effects of the bridge deck. In Section 4, the details on LBS identification using GP metamodel-based model updating are given. In Section 5, the initial LBS bounds are determined from the regression coefficients which are obtained using one-year monitoring data. The bounds are then used for the GP model updating [25, 26] to identify the LBS of Jiangyin Suspension Bridge. Finally, the conclusions of this work are drawn in Section 6.

2 Jiangyin Suspension Bridge and statistical analysis

2.1 Jiangyin Suspension Bridge

The Jiangyin Suspension Bridge has a main span of 1385 m striding the Yangtze River. The main span has a welded streamlined constant depth steel box girder of 3 m high and 36.9 m wide, which utilizes the asphalt concrete pavement and has a navigation clearance of 50 m. The bridge has two reinforced concrete towers of 190 m high and two main cables anchored in the gravity anchorages. The Jiangyin Bridge is of single-span and the bearings in the ends of the bridge deck provide vertical support only. Therefore, the bridge deck can move freely in the longitudinal direction.

A SHM system was designed and installed on the bridge in 2005, which consists of about 170 sensors including 20 accelerometers (AS), 116 Fiber Bragg grating sensors (FBG), 4 displacement

sensors (DIS), 9 global positioning system (GPS) receivers, and a number of shear pins, ultrasonic anemometers, etc. The sensors are distributed in nine equidistant cross sections (Nos. 1 ~ 9), as shown in Figure 1. The 4 draw-wire DIS (denoted as DIS_NE, DIS_NW, DIS_SE, and DIS_SW in Figure 2) were installed on both ends of the bridge deck to monitor the longitudinal displacements. One end of the DIS is fixed on the beam of the tower, and the other end on the main beam of the deck. The sampling frequencies of the DIS and the FBGT are 50 Hz and 1.1 Hz, respectively.

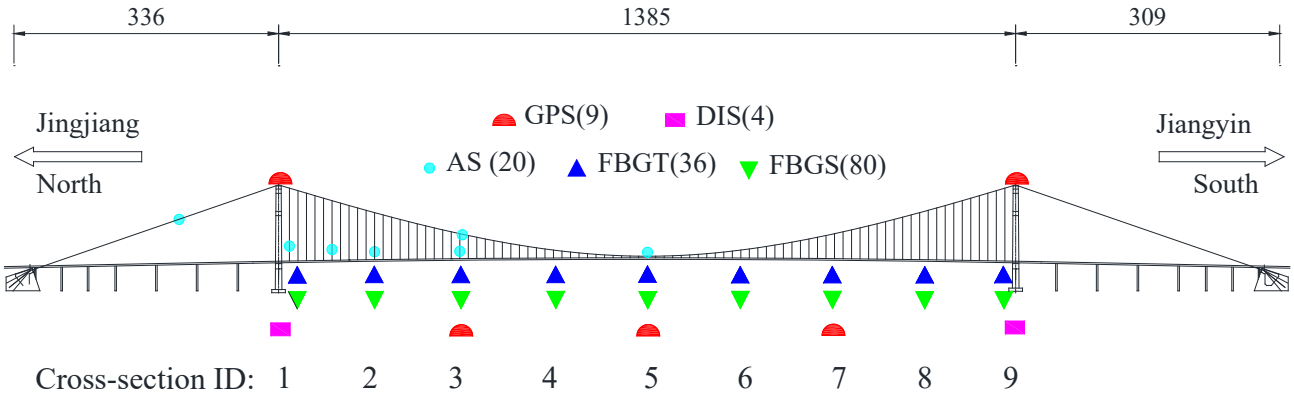

(a) Overall sensor layout (unit: m)

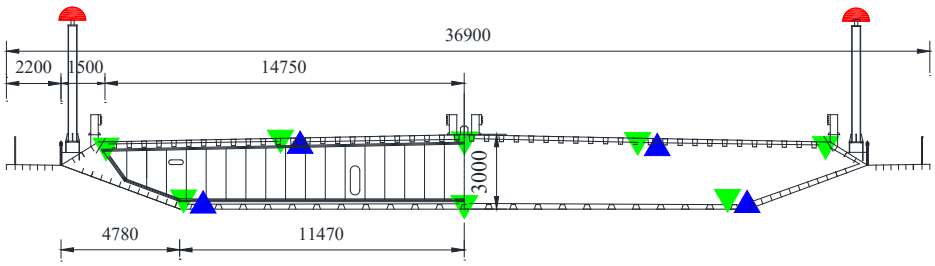

(b) Sensor layout in one cross section (unit: mm)

Figure 1. Sensor layout of the Jiangyin Suspension Bridge.

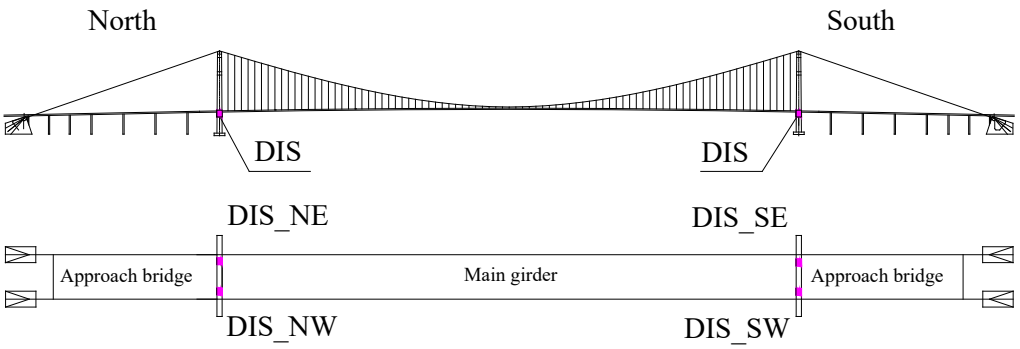

(a) Location of displacement transducers

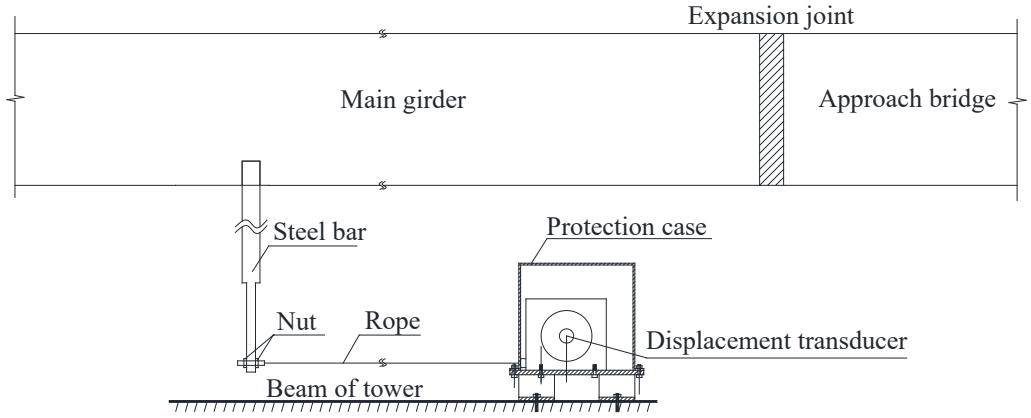

(b) Configuration of displacement transducers (DIS_SW)

Figure 2. Displacement transducer at the ends of bridge deck.

2.2 Statistical analysis of temperature-longitudinal displacement relationship

One-year monitoring data during 1 Dec 2005 ~ 30 Nov 2006 is available for investigating the relationship between temperature and longitudinal displacement. The data on 20 May 2006 is shown in Figure 3, in which the effective temperature of the bridge deck is used. In the early morning of 0:00 ~ 7:00, the structural temperature and longitudinal displacement of the beam end had no significant change. During the period of 7:00 ~ 16:00, due to the solar radiation effect, the effective temperature of the structure raised from 19.9 ºC to 41.7 ºC, and the longitudinal displacement of the 4 expansion joints decreased by 0.19 m, indicating that the bridge deck expanded and the gap of the expansion joints became smaller. From 16:00 to 24:00, the decrease in temperature caused the bridge

deck to contract and the gap of the expansion joints became larger. It is concluded from Figure 3 that the longitudinal deformation of the expansion joints is mainly caused by the temperature change.

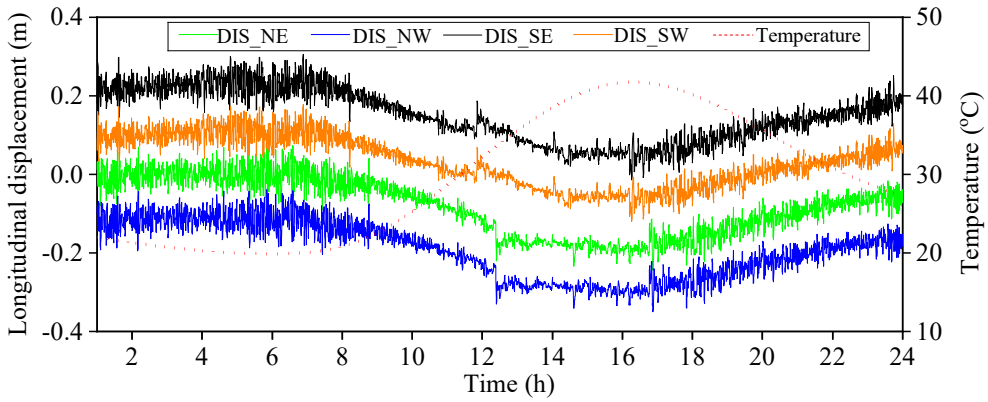

Figure 3. Longitudinal displacement of expansion joints with respect to temperature on one day (20 May 2006).

The hourly mean temperature and longitudinal displacement monitoring data in one-month period (20 May ~ 19 June 2006) are illustrated in Figure 4. When the daily temperature change was small (for example, may be a cloudy day), the displacement variations were small as well. When the daily temperature change was relatively large, the displacement variations were significant. Moreover, the longitudinal displacements of the four DISs changed with temperature consistently.

Furthermore, the seasonal variation in the hourly mean temperature and longitudinal displacement data are shown in Figure 5. The longitudinal displacements have a similar variation pattern as the seasonal temperature. The maximum longitudinal displacement and maximum temperature occurred in July and August. The longitudinal displacement caused by the seasonal temperature change can reach up to 0.5 m, more than that caused by the daily temperature variation.

The regression analysis (one-month monitoring data from 20 May to 19 June 2006 for demonstration) is then adopted to qualitatively determine the relationship between temperature and

144 longitudinal displacement. In order to better compare the correlation of the four displacement meters
145 with temperature, the initial value of the displacement is normalized to zero. The results of the four
146 joints are presented in Figure 6. The temperature and longitudinal displacement have a linear
147 relationship and the sensitivities of the four longitudinal displacements to the temperature,
148 determined by the slope of the lines, are almost the same. The slopes of the lines are not only
149 associated with the structural configuration, but also the stiffness of the expansion joints, which is
150 equivalent to the LBS and will be investigated in following sections.
151

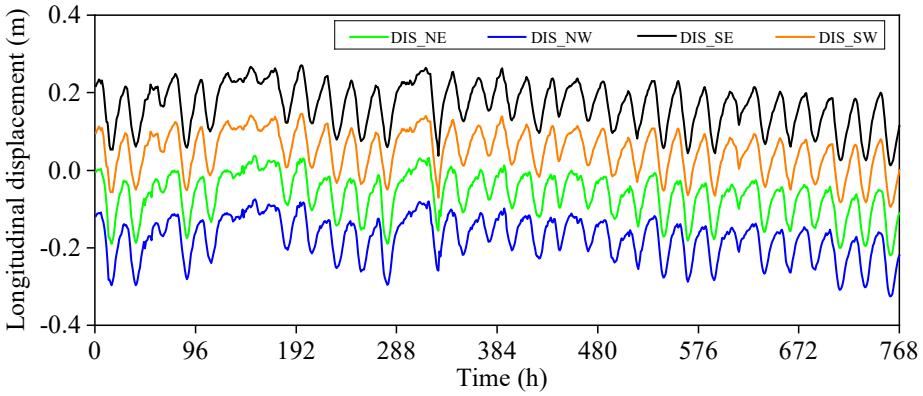

(a) Four longitudinal displacement curves

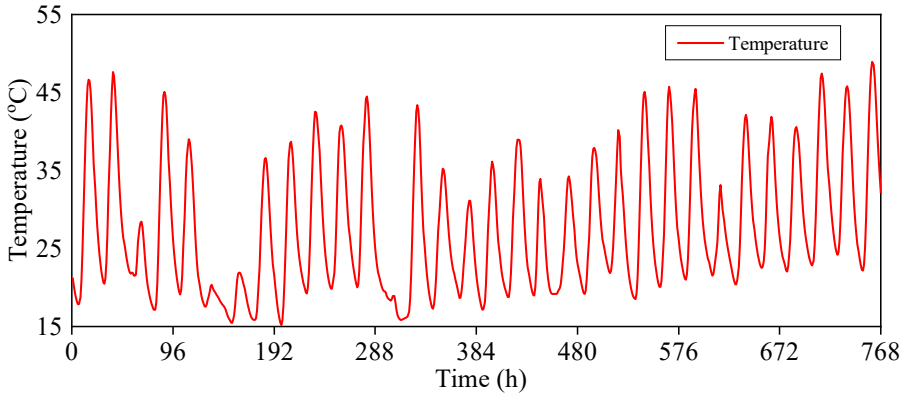

(b) Temperature curve

Figure 4. Longitudinal displacement of expansion joints with respect to temperature in one-month period (20 May ~ 19 June 2006).

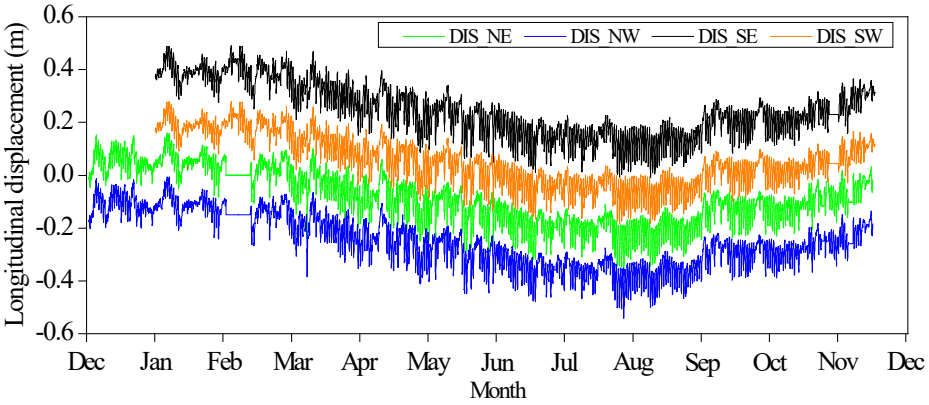

(a) Four longitudinal displacement curves

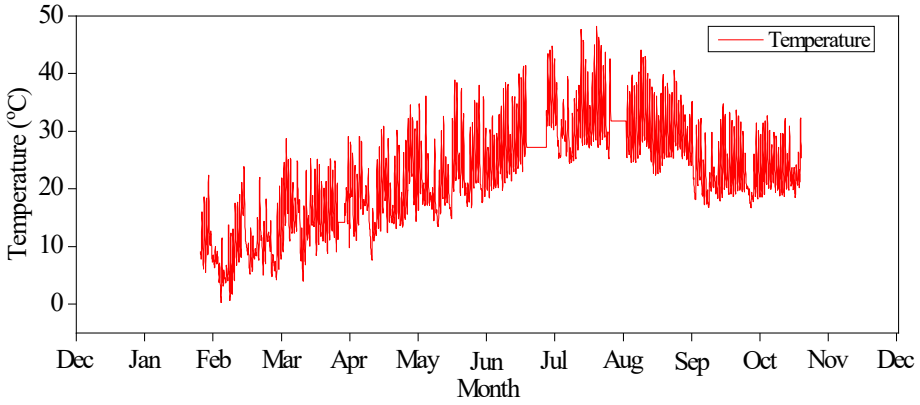

(b) Temperature curve

Figure 5. Longitudinal displacement of expansion joints with respect to temperature in one-year period (1 Dec 2005 ~ 30 Nov 2006).

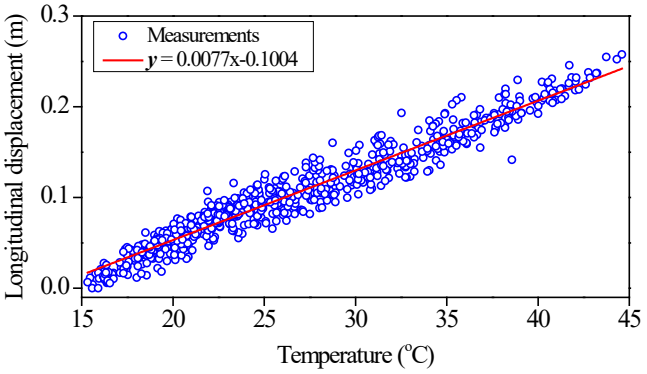

(a) North-east expansion joint

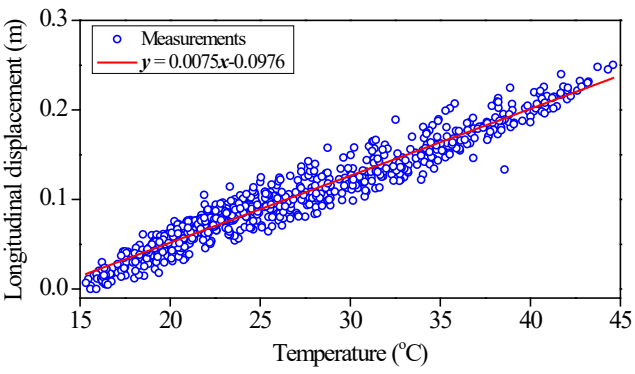

(b) North-west expansion joint

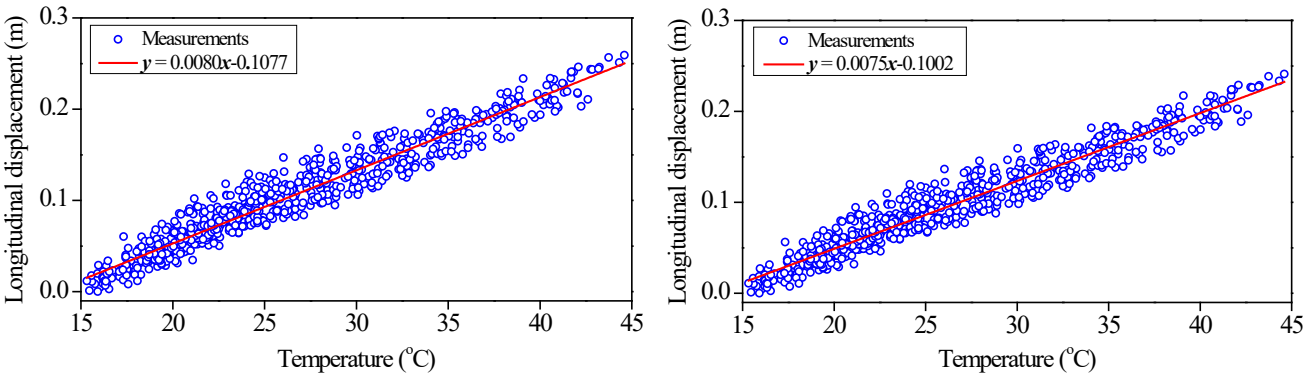

(c) South-east expansion joint (d) South-west expansion joint

Figure 6. Linear regress analysis of temperature and longitudinal displacement of expansion joints.

3 LBS formula derivation and calculation

The thermal behavior of the bridge deck can be schematically represented as shown in Figure 7, in which the bridge deck is simplified as a simple beam with two roller supports and the longitudinal constraints simulated by 4 springs at the ends. The longitudinal deformation of the bridge deck satisfies the Hooke's law, that is,

$$F = \delta_N K_N = \delta_S K_S \tag{1}$$

where F is the restrained force exerted at the bridge deck; δ_N and δ_S are the displacements of the north and south ends of the bridge deck, respectively; and K_N and K_S are the LBS of the north and south ends of the bridge deck, respectively.

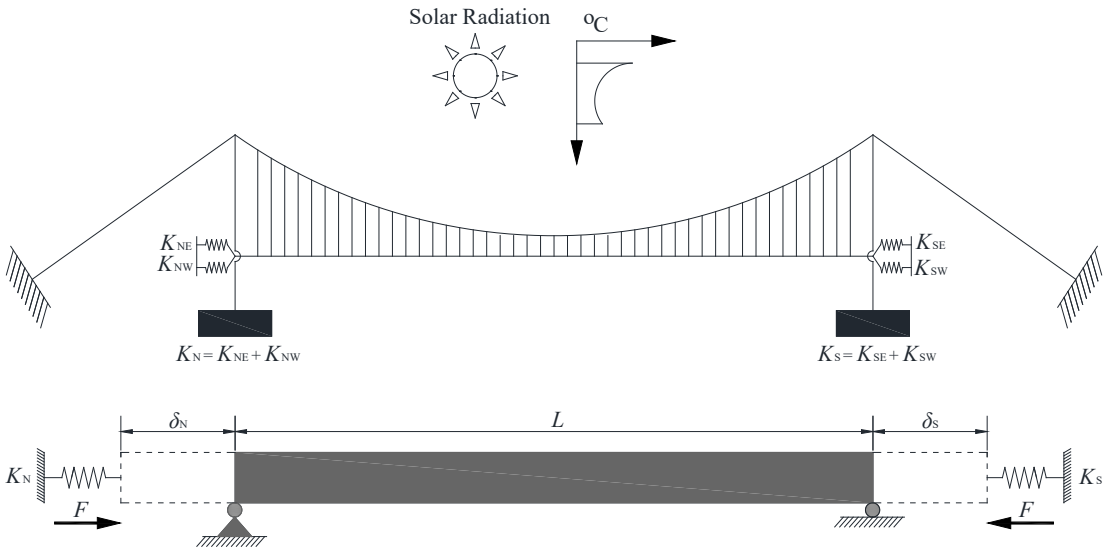

Figure 7. Schematic thermal behavior of the bridge deck.

161

162 The relationship between temperature and displacement satisfies,

$$\alpha \Delta T L = \varepsilon L + \delta \tag{2}$$

163 where α is the thermal expansion coefficient; ΔT is the variation in the effective temperature of the
164 structure; L is the length of the main span (1385 m); $\delta = \delta_N + \delta_S$ is the total longitudinal
165 displacement at the expansion joints; and ε is elastic strain of the bridge deck and can be calculated
166 from the restrained force as,

$$\varepsilon = \frac{F}{EA} \tag{3}$$

167 where E is the elastic modulus; and A is the cross-sectional area of the deck.

168 Substituting Equation (3) into Equation (2) yields,

$$\alpha \Delta T L = \frac{F}{EA} L + \left(\delta_N + \delta_S \right) \tag{4}$$

169 According to Equations (1) and (4), the LBS of the north and south ends of the bridge deck can
170 be obtained as,

$$K_N = \frac{EA}{L}\left[\alpha L\left(\frac{\Delta T}{\delta_N}\right) - \left(\frac{\delta_S}{\delta_N} + 1\right)\right] \quad (5)$$

$$K_S = \frac{EA}{L}\left[\alpha L\left(\frac{\Delta T}{\delta_S}\right) - \left(\frac{\delta_N}{\delta_S} + 1\right)\right] \quad (6)$$

171 From these formulas above, the LBS can be calculated using the monitoring data ΔT, δ_S and δ_N.
172 Furthermore, the calculated LBS need to be calculated and verified.

173 The day 15 April 2006 as an example is selected for the LBS calculation. According to
174 Equations (5) and (6), the two main values should be determined, one is $\Delta T/\delta$, the other is δ_S/δ_N (or
175 δ_N/δ_S). The former is shown in Figure 8. Figures 8(a) and (b) show that the relationship between the
176 longitudinal displacement and temperature at the north side presents an elliptic curve in daily
177 variation. The $\Delta T/\delta$ values at the downstream and upstream of the north side are 141.1 and 138.3,
178 respectively. Figures 8(c) and (d) show that the relationship between the longitudinal displacement
179 and temperature at the south side displays an overlap curve in daily variation. The $\Delta T/\delta$ values at the
180 downstream and upstream of the south side are 135.1 and 138.9, respectively. δ_{SE}/δ_{NE}, δ_{SW}/δ_{NW},
181 δ_{NE}/δ_{SE} and δ_{NW}/δ_{SW} are 1.045, 1.0006, 0.9569, and 0.9994, respectively. Based on Equations (5) and
182 (6), the LBS values are calculated as $k_{NE} = 6.54\times10^6$ *N*/*m*, $k_{NW} = 7.02\times10^6$ *N*/*m*, $k_{SE} = 6.26\times10^6$ *N*/*m*,
183 $k_{SW} = 7\times10^6$ *N*/*m*. The above analysis indicates that the LBS of four locations are slightly different.
184 And then, the estimated LBSs are applied to the 3D FEM for temperature-induced longitudinal
185 calculation.

186

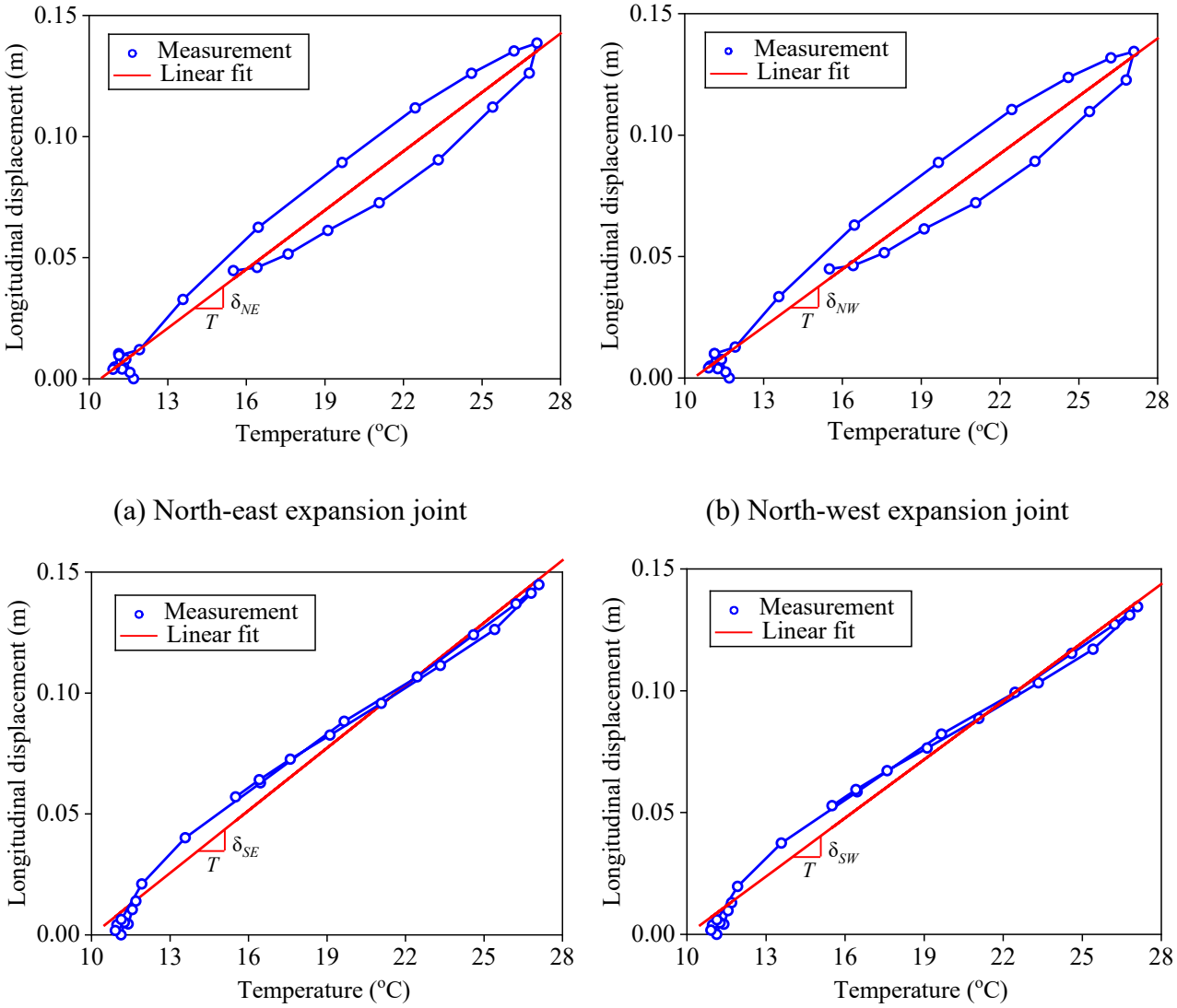

(a) North-east expansion joint

(b) North-west expansion joint

(c) South-east expansion joint

(d) South-west expansion joint

Figure 8. Displacement vs. temperature of the bridge deck on 15 April 2006.

187

188 The FEM of Jiangyin Suspension Bridge is constructed in ANSYS [27] software. The main cables,
189 hangers, and towers are modeled using link elements and the steel-box girder is simulated using
190 elastic shell elements. The ends of main cables and the bottom of towers are completely restrained.
191 The resulting FEM consists of a total of 37,276 nodes and 23,070 elements, as shown in Figure 9(a).
192 The mass density and elastic modulus of the steel and concrete is 7800 kg/m^3 , 2550 kg/m^3, 2.1×10^5
193 MPa and 3.3×10^4 MPa, respectively.

The boundary conditions at the end of the expansion joints are simulated using the 3D linear spring element (Combin14 element). One end of the spring is connected to the bridge deck, and the other end is connected to the reference points, which are fixed. The calculated LBSs of k_{NE} = 6.54×10^6 N/m, k_{NW} = 7.02×10^6 N/m, k_{SE} = 6.26×10^6 N/m, k_{SW} = 7×10^6 N/m are input to the Combin14 elements in end of bridge deck. Since the temperature distribution along the longitudinal direction of the deck is not uniform as shown in Figure 9(c), the main girder is divided into 9 segments, each being loading different measured temperature. On the cross section of each segment, the temperature loading is represented by the 4 distributed FBGT (Figure 9b). The rest of the members are subjected to ambient temperature because they have little effect on the longitudinal displacement of the main beam. During the solution process, 3600 seconds are defined as a substep, resulting in a total of 24 sets for one day. It takes about 20 minutes to solve the 24-hour temperature field change. The computer configuration is Intel(R) Core(TM) i7-4790 CPU @3.60 GHz and RAM 24.0 GB. Obviously, this calculation process is extremely time-consuming if the substep size becomes smaller. Finally, the thermal analysis [28] is conducted by applying the measured temperature data on the refined 3D FEM. The associated longitudinal displacements of the expansion joints are calculated and will be compared with measured values.

The FEM-calculated longitudinal displacements using estimated LBS mentioned above are shown in Figure 10, in which the measurements are also presented for comparison purpose. Although the two sets of displacement have similar variation pattern, their magnitudes are different, especially the peaks. The discrepancy may be due to: one is that the temperature distribution of the suspension bridge is complicated, and a limited number of sensors cannot capture the temperature behavior of the whole bridge; the other is that the LBS are calculated based on a simplified model. Therefore, it

is necessary to identify the accurate LBS values by minimizing the discrepancy between the FEM-calculated and measured longitudinal displacements. The LBS identification can be achieved by FEM updating procedure detailed in the subsequent section.

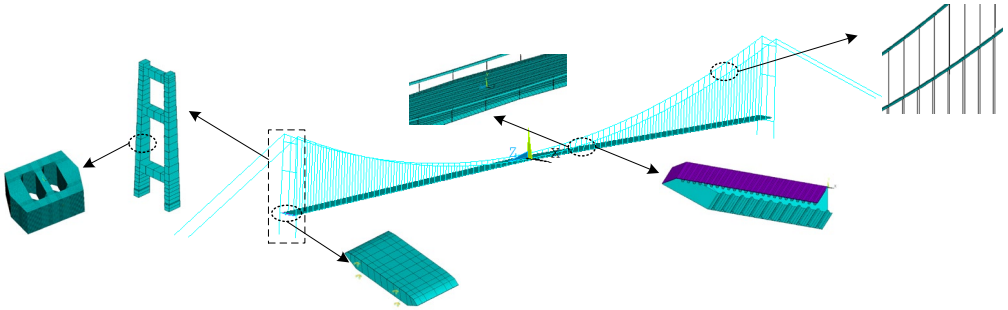

(a) A refined FEM

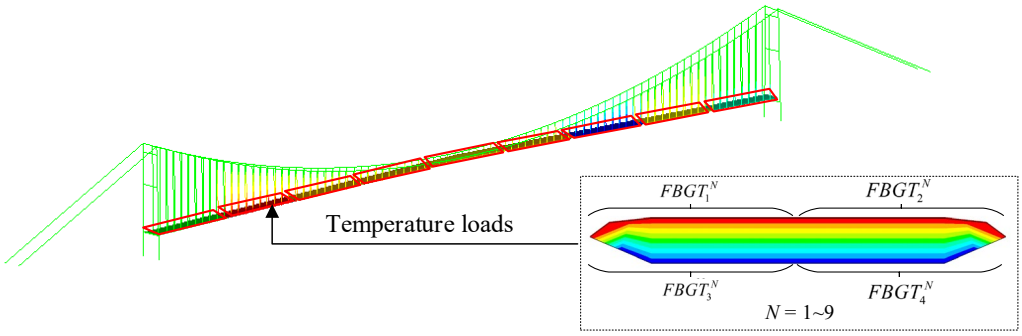

(b) Temperature field analysis

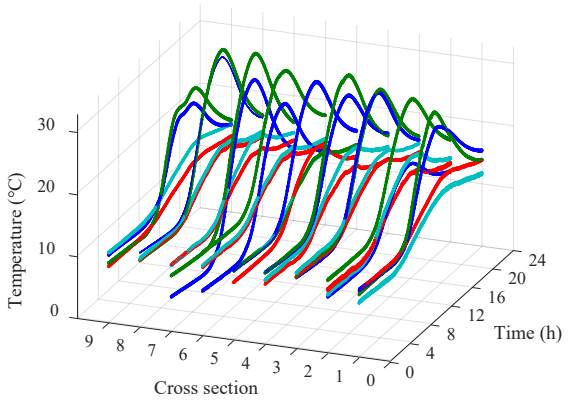

(c) Measured temperature on each cross section

Figure 9. Finite element modeling and analysis of the Jiangyin Suspension Bridge.

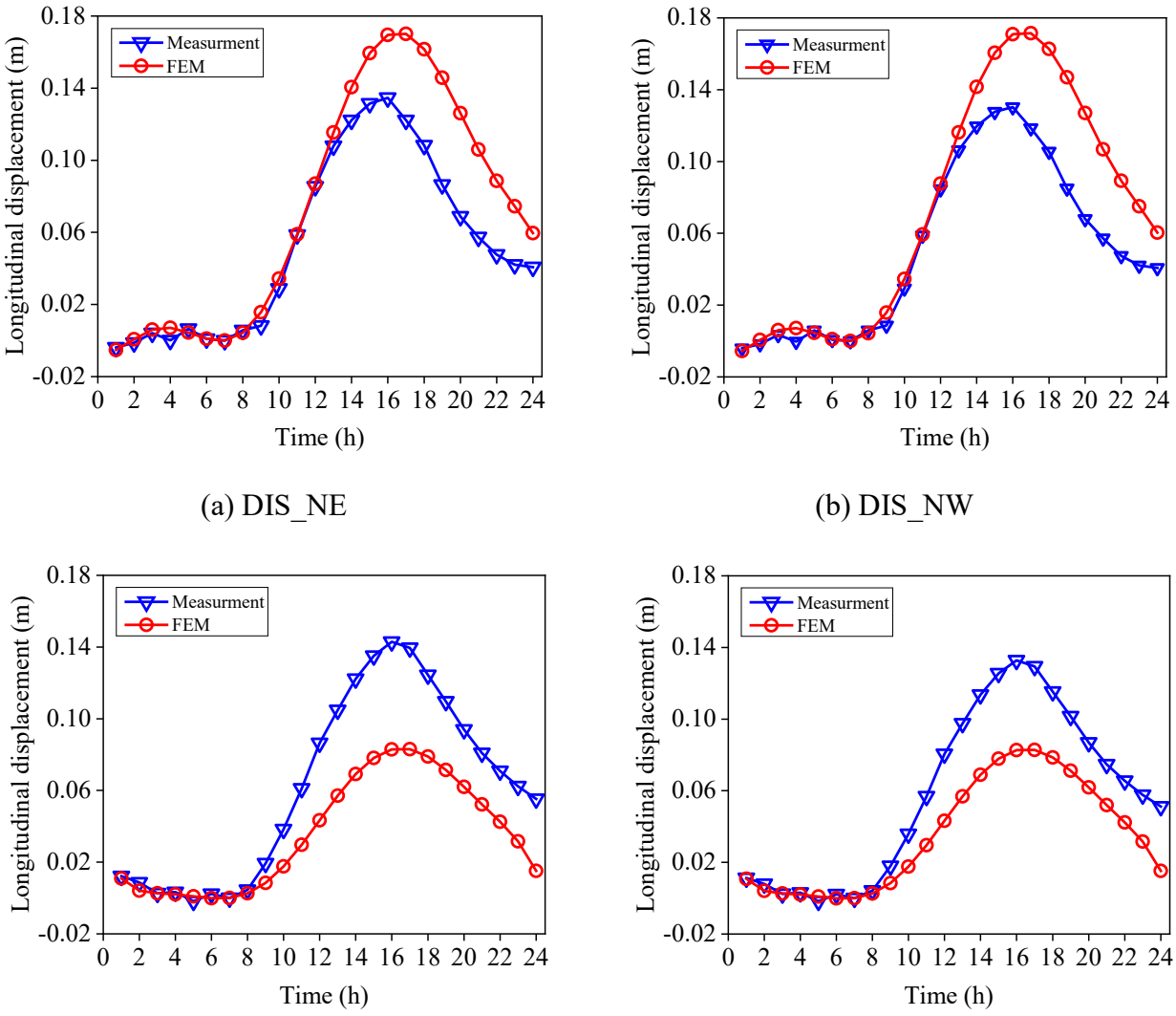

Figure 10. Calculated and measured longitudinal displacements due to temperature variation.

220

221 **4 LBS identification using metamodel-based model updating**

222 **4.1 Gaussian process metamodel**

223 The LBS identification of Jiangyin Suspension Bridge based on the FEM updating suffers from
224 the high computational cost. To reduce the computational burden, the GP metamodel is used to map
225 the relationship between the LBS and the longitudinal displacements under the thermal effects. GP
226 metamodel [29-31] is fully characterized by the mean and covariance functions. In the following, it

considers the zero-mean function and squared exponential covariance function [32] expressed by

$$C(\mathbf{x},\mathbf{x}') = \eta^2 \exp\left[-\frac{1}{2}\sum_{k=1}^{d}\left(\frac{x_k - x_k'}{\ell_k}\right)^2\right] \tag{7}$$

where x_k and x_k' are the kth component of $\mathbf{x}$ and $\mathbf{x}'$, respectively; d is the length of $\mathbf{x}$; η^2 is the signal variance; and ℓ is the characteristic length scale.

Consider an n-pair training data set $\mathcal{D} = \{\mathbf{X},\mathbf{Y}\}$, where $\mathbf{X} = \{\mathbf{x}_i\}\big|_{i=1}^{n}$ and $\mathbf{Y} = \{y_i\}\big|_{i=1}^{n}$, and y_* denotes the latent function realization to be predicted at an untried point $\mathbf{x}_*$. Using the Gaussian prior assumption that the function realizations follow the Gaussian distribution, one has

$$\mathbf{Y} \sim \mathcal{N}(\mathbf{0},\mathbf{C}) \tag{8}$$

$$\begin{bmatrix}\mathbf{Y}\\ y_*\end{bmatrix} \sim \mathcal{N}\left(\begin{bmatrix}\mathbf{0}\\ 0\end{bmatrix},\begin{bmatrix}\mathbf{C} & \mathbf{C}_*\\ \mathbf{C}_*^{\top} & \tilde{C}\end{bmatrix}\right) \tag{9}$$

where $\mathbf{C} = C(\mathbf{X},\mathbf{X})$; $\mathbf{C}_* = C(\mathbf{x}_*,\mathbf{X})$; $\tilde{C} = C(\mathbf{x}_*,\mathbf{x}_*)$; and $(\bullet)^{\top}$ represent the transpose operator.

Applying Bayes' rule, the joint posterior distribution of y_* conditioned on the training data set $\mathcal{D}$ is also Gaussian, in the expression of

$$y_* \sim \mathcal{N}\left(\mu_{y_*},\sigma_{y_*}^2\right) \tag{10}$$

with the mean and variance given by

$$\mu_{y_*} = \mathbf{C}_*\mathbf{C}^{-1}\mathbf{Y} \tag{11}$$

$$\sigma_{y_*}^2 = \tilde{C} - \mathbf{C}_*^{\top}\mathbf{C}^{-1}\mathbf{C}_* \tag{12}$$

Due to the adoption of the zero-mean function, the covariance function parameters $\Theta = \{\ell_1,\ldots,\ell_d,\eta^2\}$, usually termed as hyperparameters in the machine learning community, completely govern the GP metamodel. In the Bayesian context, the hyperparameters are commonly estimated by maximizing the marginal likelihood of the training data. For computational convenience, the estimation of the hyperparameters is converted to minimization of the negative

242 logarithmic marginal likelihood (NLML). The NLML, $\mathcal{L}(\boldsymbol{\Theta})$, and its partial derivatives with respect

243 to the hyperparameters $\boldsymbol{\Theta}$ have closed-form expressions as follow

$$\mathcal{L}(\boldsymbol{\Theta}) = \frac{1}{2}\mathbf{Y}^{\top}\mathbf{C}^{-1}\mathbf{Y} + \frac{1}{2}\log|\mathbf{C}| + \frac{n}{2}\log(2\pi) \tag{13}$$

$$\frac{\partial \mathcal{L}(\boldsymbol{\Theta})}{\partial \boldsymbol{\Theta}_i} = \frac{1}{2}\mathrm{tr}\left(\mathbf{C}^{-1}\frac{\partial \mathbf{C}}{\partial \boldsymbol{\Theta}_i}\right) - \frac{1}{2}\mathbf{Y}^{\top}\mathbf{C}^{-1}\frac{\partial \mathbf{C}}{\partial \boldsymbol{\Theta}_i}\mathbf{C}^{-1}\mathbf{Y} \tag{14}$$

244 where $|\bullet|$, $\mathrm{tr}(\bullet)$, and $(\bullet)^{\top}$ represent the determinant, trace, and transpose operators, respectively.

245

246 **4.2 Objective function and optimization**

247 The LBS identification is performed through the GP metamodel-based model updating. Model

248 updating is a process of calibrating structural parameters, so that the calibrated FEM can better

249 reflect the observed data [33]. It is essentially a mathematical optimization problem of finding the

250 global minimum of an objective function that defines the difference between the analytical and

251 experimental responses. In this study, the objective function is formulated as a sum of the relative

252 differences between the analytical and measured longitudinal displacements,

$$\Pi(\mathbf{x}) = \sum_{j=1}^{k} \frac{\left\|\hat{\mathbf{y}}_j(\mathbf{x}) - \mathbf{y}_j\right\|_2^2}{\left\|\mathbf{y}_j\right\|_2^2} \tag{15}$$

253 where $\mathbf{x}$ is the LBS to be updated, $\hat{\mathbf{y}}_j(\mathbf{x})$ represents the GP predicted longitudinal displacement at

254 the *i*th position; $\mathbf{y}_j$ is the corresponding measurement; and $\|\bullet\|_2$ denotes 2-norm operator.

255 Subsequently, the LBS identification can be posed as a constrained minimization problem of

256 objective function $\Pi(\mathbf{x})$, such that

$$\begin{aligned} &\hat{\mathbf{x}} = \arg\min_{\mathbf{x}} \Pi(\mathbf{x}) \\ &\text{s.t.} \quad \underline{\mathbf{x}} \le \mathbf{x} \le \overline{\mathbf{x}} \end{aligned} \tag{16}$$

257 where $\underline{\mathbf{x}}$ and $\overline{\mathbf{x}}$ stand for the lower and upper bounds of the LBS, respectively. The whole

optimization process does not involve the computationally demanding FEM owning to the use of the GP metamodel. As such, the above optimization problem can be readily solved using the available optimization techniques. Here the numerical software MATLAB is adopted, and *fmincon* function is used as the optimization solver to search the minimum of the objective function. The resultant optimal parameters are considered as the LBS of the Jiangyin Bridge.

5 LBS identification of the Jiangyin Suspension Bridge

5.1 Initial LBS bounds

One-year monitoring data from 1 Dec 2005 to 30 Nov 2006 is used to determine the initial LBS bounds. Due to lack of data, only 244 days of data can be used for regression analysis. A total of 244 regression lines are obtained and plotted in the left column of Figure 11. To have a clear picture of all $\Delta T / \delta$ values, they are plotted in the right plane of Figure 11. From Equations (5) and (6), the approximate LBS values averaged over 244 values are estimated as $k_{NE} = 3.5\times10^{6}$ N/m, $k_{NW} = 7.1\times10^{6}$ N/m, $k_{SE} = 2.1\times10^{6}$ N/m, and $k_{SW} = 6.1\times10^{6}$ N/m, respectively. The range bounds of LBS are determined as $k_{NE} \in \left[0, 6.7\times10^{7}\right]$, $k_{NW} \in \left[0, 8\times10^{7}\right]$, $k_{SE} \in \left[0, 5.2\times10^{7}\right]$, and $k_{SW} \in \left[0, 6\times10^{7}\right]$, respectively. The determined range bounds of LBS will used be set as the lower and upper bounds of **x** in Equation (16).

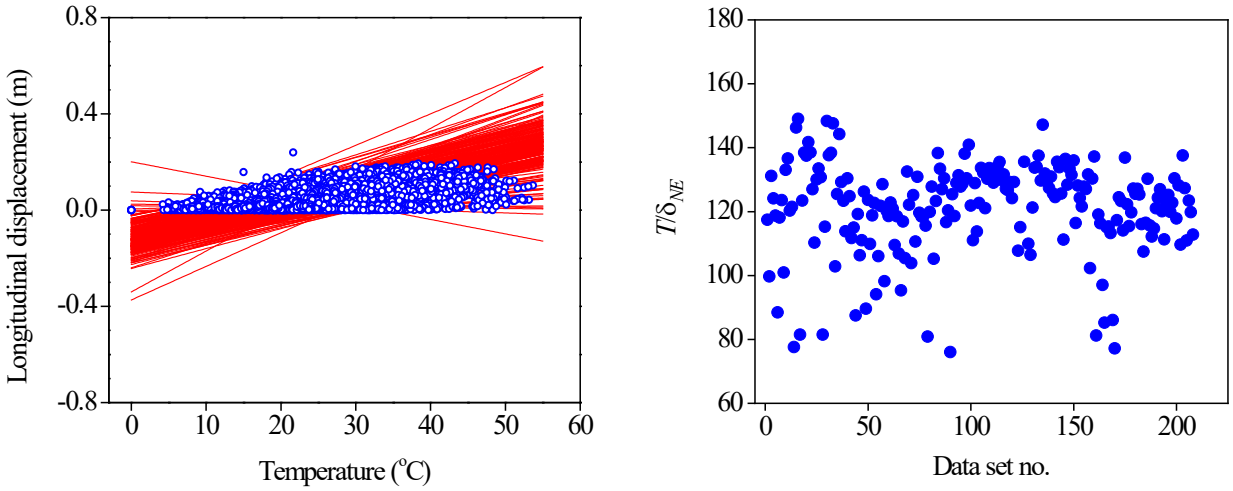

(a) DIS_NE

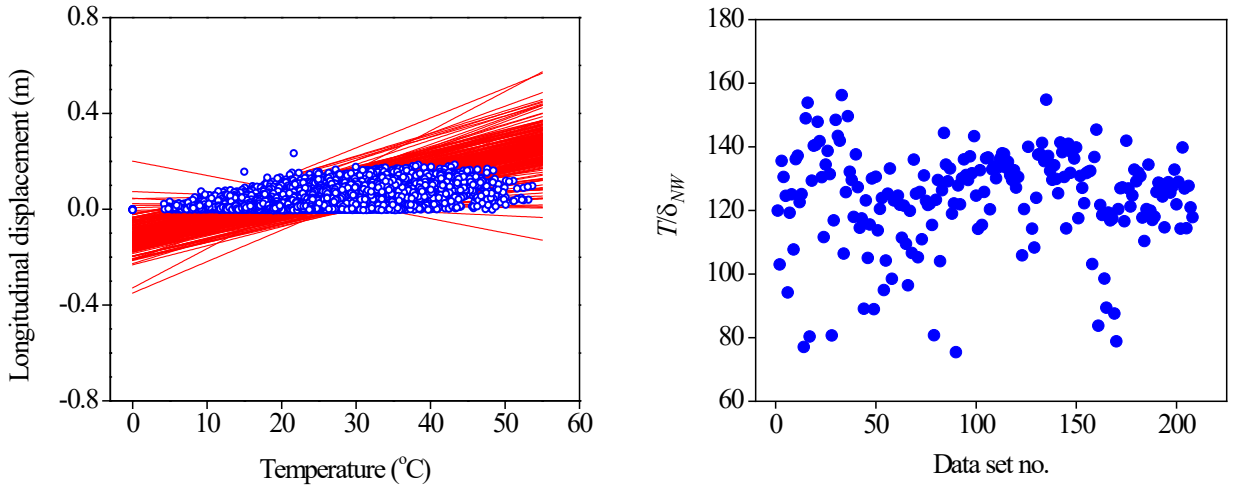

(b) DIS_NW

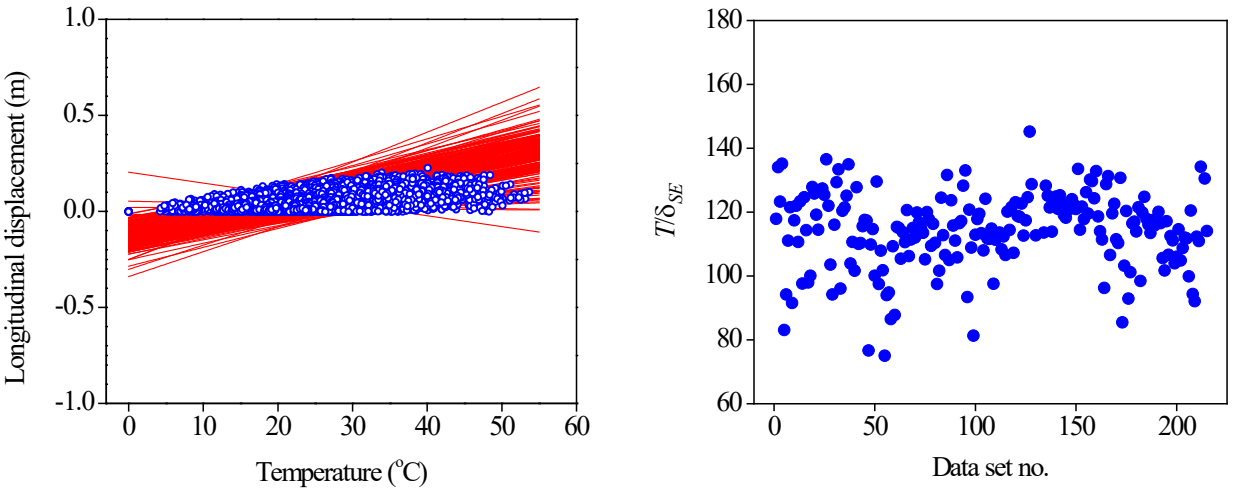

(c) DIS_SE

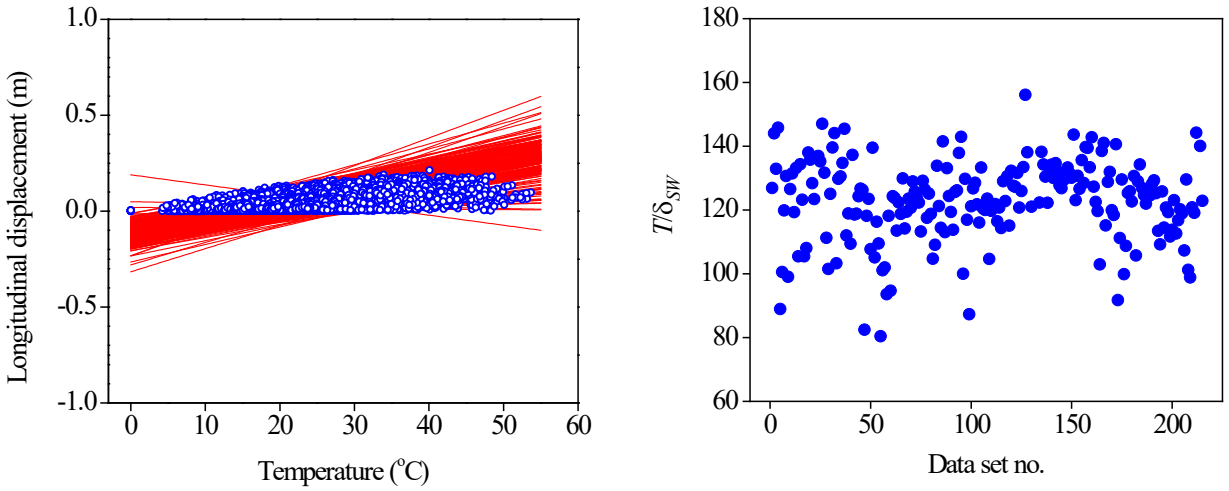

(d) DIS_SW

Figure 11. Displacement vs. temperature of the bridge deck from 1 Dec 2005 to 30 Nov 2006.

275

276 **5.2 Construction of the GP metamodel**

277 Construction of the GP metamodel consists of training data generation, hyperparameter
278 estimation, and model validation. The specific implementation process is given as follows:

279 1. The Sobol sequence sampling is adopted for the experimental design to generate input samples
280 since it owns an attractive low-discrepancy feature [34]. The generated Sobol points fall in a unit
281 hypercube and thus need to be transformed into the real physical space of the LBS, that is, the
282 initial bounds of k_{NE}, k_{NW}, k_{SE}, k_{SW} determined in the above section.

283 2. The hourly mean temperature monitoring data is then selected as the input loads on the refined
284 FEM. The temperature data are applied to the 3D FEM for thermal analysis to calculate the
285 associated longitudinal displacements. The thermal analysis is repeated for each time instant.
286 Then the longitudinal displacement array is obtained. Then, the generation of training data,
287 which is composed of the LBSs and the obtained longitudinal displacement, is completed.

288 3. The obtained input-output (LBS and longitudinal displacement) pairs are regarded as training
289 data for construction of the GP metamodel. As mentioned earlier, the hyperparameters

completely determine the GP metamodel. The hyperparameters are estimated from the training data by minimizing the NLML. To avoid getting stuck in the local minima during the optimization, the multi-starting point strategy-assisted optimization solver is utilized to infer the optimal hyperparameters.

4. The model validation process is conducted to check the accuracy of the constructed GP metamodel using the leave-one-out cross-validation (LOOCV) technique. The validated GP metamodel is used as the surrogate of the FEM for the subsequent LBS identification.

5.3 LBS identification

Since the FEM-derived longitudinal displacements are approximated by the constructed GP metamodel, the optimization procedure for identification of the LBS is computationally efficient. Subsequently, the metamodel-based model updating is adopted. Following the implementation procedure detailed in Section 4.2, the optimal LBS is identified by minimizing the difference between the analytical and measured longitudinal displacements defined by Equation (16). The results are $k_{NE} = 3.37 \times 10^6$ N/m, $k_{NW} = 5.12 \times 10^6$ N/m, $k_{SE} = 3.37 \times 10^6$ N/m, and $k_{SW} = 4.25 \times 10^6$ N/m. The longitudinal displacements on 25 May 2006 are selected to verify the LBS identification results. The comparison of updated FEM-derived and measured longitudinal displacements is shown Figure 12, exhibiting a good agreement.

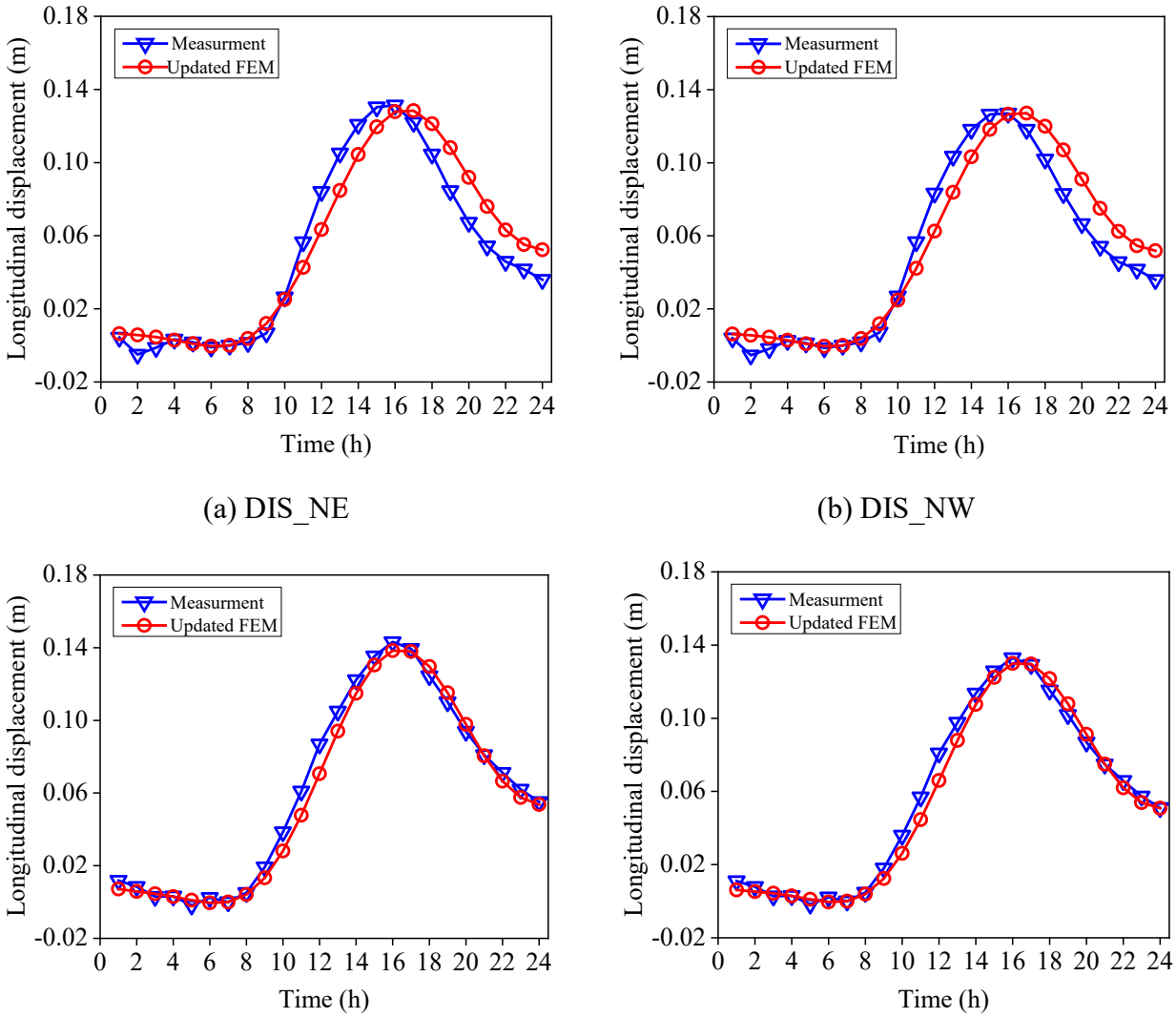

(a) DIS_NE (b) DIS_NW

(c) DIS_SE (d) DIS_SW

Figure 12. FEM-derived and measured longitudinal displacements under temperature loading after calibration.

Further, the updated LBS values are also applied to one day (20 April 2007) beyond the used one-year period. The predicted and measured longitudinal displacements on the day are compared in Figure 13, also showing a good agreement. It should be noted that lag between the updated FEM lines and the measurement lines shown in Figures 12 and 13 may be because the time delay may occur on the temperature and displacement signals. The lag phenomenon was also reported by Guo et

al. [15]. The calculated displacement has a little error when temperature rises. This may be because the FEM does not consider the wind and traffic loads. In line with above observations, it can be concluded that the identified LBS is able to reflect the real condition of the bridge expansion joints.

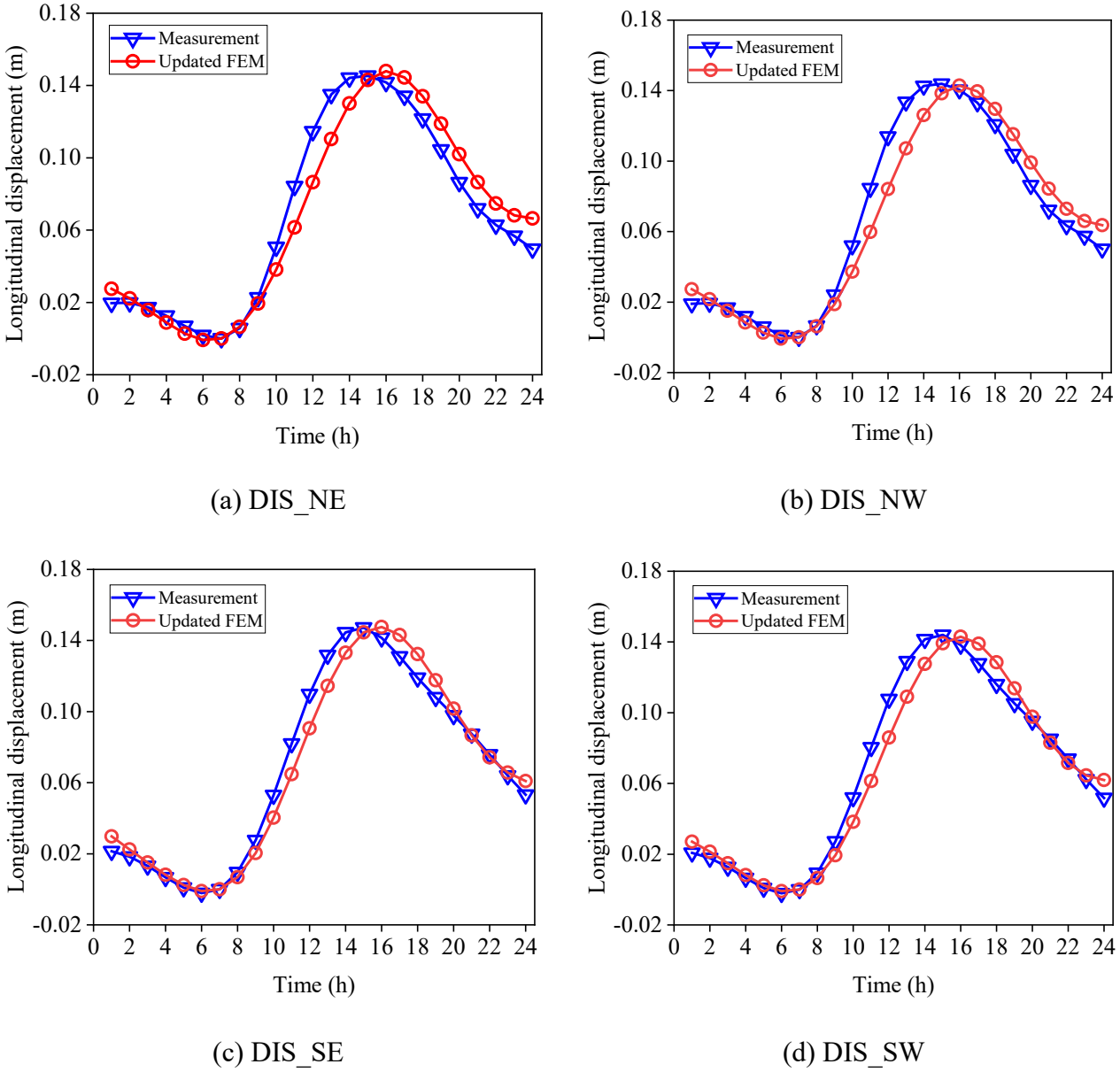

(a) DIS_NE (b) DIS_NW

(c) DIS_SE (d) DIS_SW

Figure 13. Assessment of prediction performance of the calibrated FEM using identified LBS.

6 Conclusions

The bridge expansion joints suffer damage more frequently than other structural components,

especially for a long-span bridge. Destructive bridge expansion joints not only cause discomfort in driving, but also change the mechanical characteristics of the bridge structure. So, it is important to assess the condition of the bridge expansion joints. However, traditional FEM updating technology requires a large computational cost and time-consuming. Therefore, this study presents an efficient metamodel-based model updating method for the LBS identification of a long-span suspension bridge using the long-term displacement and temperature measurements. The main conclusions of this study are summarized as follows:

(1) Jiangyin Suspension Bridge as an example for LBS research. The temperature and longitudinal displacement have a linear relationship and the sensitivities of the four longitudinal displacements to the temperature, determined by the slope of the lines, are almost the same. The slopes of the lines are not only associated with the structural configuration, but also the stiffness of the expansion joints, which is equivalent to the LBS.

(2) The relationship among the boundary stiffness, structural temperature and longitudinal displacement is formulated using the thermal effect mechanism. The reasonable LBS bounds are determined on the one-year monitoring data. A GP metamodel as a surrogate of the refined 3D FEM for model updating and LBS identification. The calibration results show that there is improved match between the analytical and measured longitudinal displacements. Moreover, the prediction performance of the calibrated FEM using the accurate LBS is explored. The predicted longitudinal displacements also exhibit a good agreement with the measurements. Therefore, it is concluded that the identified LBS is sufficiently accurate and can reflect the real condition of the bridge expansion joints. It is verified that the GP metamodel-based model updating method is effective for LBS identification of long-span bridges.

Acknowledgement

This research was financially supported by the National Natural Science Foundation of China (51878235 and 51778204) and General Research Found (Project No. PolyU 152125/17E) of RGC, Hong Kong. Dr. Yufeng Zhang of Jiangsu Transportation Institute (JSTI) is greatly appreciated for providing the monitoring data of the Jiangyin Suspension Bridge.

References

1. Roeder CW. Fatigue and dynamic load measurements on modular expansion joints. *Constr Build Mater*. 1998; 12(2-3), 143-150.
2. Chang LM, Lee YJ. Evaluation of performance of bridge deck expansion joints. *J. Perform Constr. Facil*. 2002; 16(1): 3-9.
3. Marques Lima J, de Brito J. Inspection survey of 150 expansion joints in road bridges. *Eng Struct.* 2009; 31(5), 1077-1084.
4. Yanev B. Joints: the weak link in bridge structures and lifecycles. *Smart Structures and Systems*, 2015; 15(3), 543-553.
5. Xia Q, Cheng YY, Zhang J, Zhu FQ. In-Service Condition Assessment of a Long-Span Suspension Bridge Using Temperature-induced Strain Data. *J. Bridge Eng* 2017, 22(3): 04016124.
6. Guo T, Huang LY, Liu J, Zou Y. Damage mechanism of control springs in modular expansion joints of long-span bridges. *J. Bridge Eng*. 2018; 23(7): 04018038.
7. Wang GX, Ye JH. Localization and quantification of partial cable damage in the long-span cable-stayed bridge using the abnormal variation of temperature-induced girder deflection. *Struct Control Health Monit*. 2018; e2281.
8. Fu Y, DeWolf JT. Monitoring and analysis of a bridge with partially restrained bearings. *J. Bridge Eng.* 2001; 6(1), 23-29.
9. Xu L, Jiang JJ, Guo JJ. Modal analysis of Humen suspension bridge. *China Civil Engineering Jouranl*. 2002; 35(1), 25-27. (In Chinese).
10. Zhou, L. R., Xia, Y., Brownjohn, J. M. W. and Koo, Y. K. Temperature Analysis of a Long-span

373 Suspension Bridge based on Field Monitoring and Numerical Simulation. *J. Bridge Eng.* 2016;
374 21 (1): 04015027.
375 11. Kromanis R, Kripakaran P and Harvey B. Long-term structural health monitoring of the Cleddau
376 bridge: evaluation of quasi-static temperature effects on bearing movements. *Structure and*
377 *Infrastructure Engineering*. 2016; 12(10), 1342-1355.
378 12. Xia Q, Zhang J, Tian YD, Zhang YF. Experimental study of thermal effects on a long-span
379 suspension bridge. *J Bridge Eng*. 2017; 22(7): 04017034.
380 13. Ni YQ, Hua XG, Wong KY, Ko JM. Assessment of bridge expansion joints using long-term
381 displacement and temperature measurement. *J. Perform Constr Facil*. 2007; 21(2), 143-151.
382 14. Ding Y, Li A. Assessment of bridge expansion joints using long-term displacement measurement
383 under changing environmental conditions. *Front. Archit. Civ. Eng*. *China*, 2011; 5(3), 374-380.
384 15. Guo T, Liu J, Zhang Y, Pan S. Displacement monitoring and analysis of expansion joints of
385 long-span steel bridges with viscous dampers. *J. Bridge Eng*. 2015; 20(9): 04014099.
386 16. Li XL, Sun LM. Condition assessment of expansion joint of a cable-stayed bridge based on
387 long-term monitoring. *Applied Mechanics and Materials*. 2012; (204-208), 2127-2134.
388 17. Huang, HB, Yi TH, Li HN, Liu H. New representative temperature for performance alarming of
389 bridge expansion joints through temperature-displacement relationship. *J. Bridge Eng*. 2018;
390 23(7): 04018043.
391 18. Winkler J, Specialist C, Hansen DH. Innovative long-term monitoring of the great belt bridge
392 expansion joint using digital image correlation, *Structural Engineering International*. 2018;
393 28(3):347-352.
394 19. Yarnold MT, Moon FL, Aktan AE. Temperature-based structural identification of long-span

bridges. *J. Struct Eng*. 2015; 141(11): 04015027.

20. Murphy B, Yarnold M. Temperature-driven structural identification of a steel girder bridge with an integral abutment. *Eng Struct*. 2018; 155:209-221.
21. Zhou S, Song W. Environmental-effects-embedded model updating method considering environmental impacts. *Struct Control Health Monit*. 2018; 25:e2116.
22. Jesus A, Brommer P, Zhu YJ, Laory I. Comprehensive bayesian structural identification using temperature variation. *Eng Struct*. 2017; 141:75-82.
23. Jesus A, Brommer P, Westgate R, Koo K, Brownjohn JMW Laory I. Bayesian structural identification of a long suspension bridge considering temperature and traffic load effects. *Structural Health Monitoring*. 2019; 18(4):1310-1323.
24. Xia Q, Zhou L, Zhang J. Thermal performance analysis of a long-span suspension bridge with long-term monitoring data. *J Civil Struct Health Monit*. 2018; 8(4):543-553.
25. Ren WX, Chen HB. Finite element model updating in structural dynamics by using the response surface method. *Eng Struct*. 2010; 32(8):2455-2465.
26. Wan HP, Ren WX. Stochastic model updating utilizing Bayesian approach and Gaussian process model. *Mechanical Systems and Signal Processing*, 2016; 70-71:245-268.
27. ANSYS 17 [Computer software]. Canonsburg, PA, ANSYS.
28. Xia Y, Chen B, Zhou XQ, Xu YL. Field monitoring and numerical analysis of Tsing Ma suspension bridge temperature behavior. *Struct. Control Health Monit.* 2013; 20:560-575.
29. Wan HP, Mao Z, Todd MD, Ren WX. Analytical uncertainty quantification for modal frequencies with structural parameter uncertainty using a Gaussian process metamodel. *Eng Struct*, 2014; 75:577-589.

30. Wan HP, Ren WX, Todd MD. An efficient metamodeling approach for uncertainty quantification of complex systems with arbitrary parameter probability distributions. *Int J Numer Meth Engng.* 2017; 109:739-760.
31. Wan HP, Todd MD, Ren WX. Statistical framework for sensitivity analysis of structural dynamic characteristics. *J. Eng Mech*. 2017; 143(9):04017093.
32. Rasmussen CE, Williams CKI. Gaussian processes for machine learning, MIT Press, Cambridge, MA, 2006.
33. Friswell MI, Mottershead JE. Finite element model updating in structural dynamics. Kluwer Academic Publishers Group, Norwell, 1995.
34. Wan HP, Ren WX. Parameter selection in finite-element-model updating by global sensitivity analysis using Gaussian process metamodel. *J. Struct Eng*. 2015; 141(6):04014164.